18 J

Inert Electrode Program

Report on the Source of the Electrochemical Impedance on Cermet Inert Anodes

February 1991

⁂ **Battelle**

On the cover:

Aluminum reduction pots at the Pittsburgh Reduction Company's (Alcoa's) plant in 1889. Adapted from a photograph, courtesy of Alcoa.

Inert Electrodes Program

REPORT ON THE SOURCE OF THE
ELECTROCHEMICAL IMPEDANCE ON CERMET INERT ANODES

C. F. Windisch, Jr.
N. D. Stice

February 1991

Pacific Northwest Laboratory
Richland, Washington 99352

PREFACE

The Inert Electrode Program at Pacific Northwest Laboratory (PNL)[a] is supported by the Office of Industrial Processes of the U. S. Department of Energy and is aimed at improving the energy efficiency of Hall-Heroult cells through the development of inert anodes. The inert anodes currently under study are composed of a cermet material of the general composition NiO-$NiFe_2O_4$-Cu. The program has three primary objectives: (a) to evaluate the anode material in a scaled-up, pilot cell facility, (b) to investigate the mechanisms of the electrochemical reactions at the anode surface, and (c) to develop sensors for monitoring anode and/or electrolyte conditions. This report covers the results of a portion of the studies on anode reaction mechanisms.

(a) PNL is operated for the U.S. Department of Energy by Battelle Memorial Institute under Contract DE-ACO6-76RLO 1830.
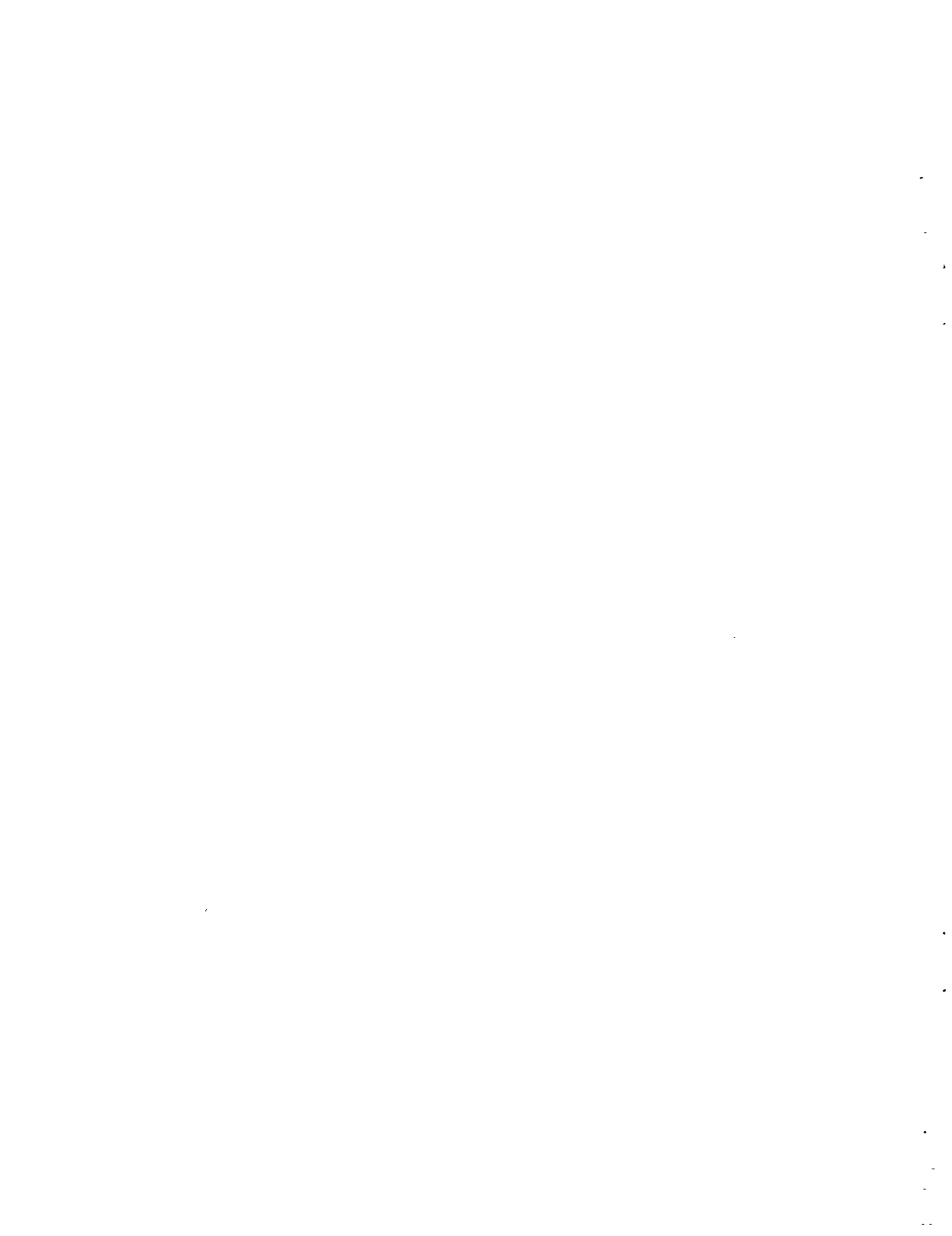
SUMMARY

The electrochemical impedances of cermet inert anodes in alumina-saturated molten cryolite as a function of frequency, current density, and time indicated that a significant component of the impedance is due to the gas bubbles produced at the anode during electrolysis. The data also showed a connection between surface structure and impedance that appears to be related to the effects of surface structure on bubble flow. Given the results of this work, it is doubtful that a resistive film contributes significantly to the electrochemical impedances on inert anodes. Properties previously assigned to such a film are more likely due to the bubbles and those factors that affect the properties and dynamics of the bubbles at the anode surface.

ACKNOWLEDGMENTS

CONTENTS

FIGURES

TABLES

1.0 INTRODUCTION

Experimental studies conducted at the Pacific Northwest Laboratory (PNL) in FY 1987, FY 1988 and early FY 1989 indicated that the cermet inert anodes evaluated by PNL exhibited a characteristic impedance during the electrolytic production of aluminum in bench-scale Hall-Heroult cells. This impedance was found to have the following characteristics (Strachan et al. 1988):

- It was largely resistive in nature.

- It varied as a function of current density, giving a minimum at about 0.5 A/cm^2.

- It appeared to depend on alumina concentration in the electrolyte. In general, the impedance seemed to increase with increasing alumina concentration.

- It exhibited a time dependence. Different anodes gave different impedances at different times after polarization.

- At high current densities (>1 A/cm^2), discontinuous changes in the impedance occurred, causing "spikes" in the current or voltage data.

Based on these characteristics, PNL originally proposed that a resistive film formed on inert anodes during electrolysis. It was argued that the formation of this film was necessary to protect the inert anode from corrosion reactions that would otherwise occur in the molten electrolyte. It was also proposed that an anodic current density of 0.5 A/cm^2 formed a film with optimum passivating-like characteristics. At lower current densities, the film was proposed to be incompletely formed, resulting in corrosion of the cermet's metallic phase. At higher current densities, it was proposed that the film would become too thick and its resistance would become too high to sustain the current density. Consequently, the film would rupture, resulting in sudden and severe corrosion at the electrode's metal phase. The rupturing events in the film were indicated by sudden drops in impedance and appeared as "spikes" in the voltage data for a cell under galvanostatic (constant current) control.

PNL also proposed that the quality of the film depended on the alumina concentration in the electrolyte. Higher alumina concentrations seemed to

1.1

favor a more resistive, presumably thicker, film. Consequently, film rupturing behavior was considered to be more likely at high alumina concentrations (close to saturation) when current densities were above 0.5 A/cm^2. Problems with reproducibility of the experimental results were encountered, however, when attempts were made to relate anode impedance explicitly to alumina concentration. It was then concluded that the film impedance was dynamic, changing with time and with small fluctuations in cell conditions.

Attempts to identify the composition of the film in FY 1988 were largely unsuccessful. Post-mortem X-ray diffraction of frozen electrolyte near the surface region showed the presence of alumina, but it was uncertain whether the alumina was part of a film or simply precipitate that formed on the anode during cool-down.

During FY 1989 and FY 1990, experiments were performed to identify the properties and composition of the film using a variety of techniques. The milestone report titled "Characterization of the Reaction Layer or Film on PNL Inert Anodes: Progress Report for April-December 1989" (Windisch and Stice 1990a) discussed the results of electrochemical impedance and potential-step studies. These results suggested that morphological characteristics of the cermet anode, specifically roughness and surface porosity, play an important role in reactions at the surface and in determining electrode impedance. These conclusions were supported by the results of microscopic and compositional analysis of the reaction zone reported in the follow-up milestone document titled "Final Report on the Characterization of the Film on Inert Anodes" (Windisch and Stice 1990b). This work indicated that an alumina film does not form to protect the cermet inert anode from dissolution. Rather, significant morphological and compositional changes occurred at or near the anode surface during polarization. These changes and the chemical changes that caused them involve the cermet material itself and appear to be responsible for some of the properties previously assigned to an alumina film.

Since the electrochemical impedance measured on the cermet inert anodes was originally attributed by PNL to the alumina film (Strachan et al. 1988), another explanation for the source of the impedance was required. The objective of the current work was to obtain more electrochemical impedance

1.2

data under a variety of conditions and on different anodes to see if any relationships could be developed among experimental parameters that might clarify the source of the anode impedance. The results of these tests, when compared with studies reported in the literature (Tobias 1959; Dewing and van der Kouwe 1975; Zuca et al. 1980) and taken together with the recent work at PNL (Windisch and Stice 1990a,b), strongly suggest that the oxygen gas bubbles produced during electrolysis provide an important contribution to the electro-chemical impedance at the anode. The impedance was also found to depend strongly on anode surface structure and on cell geometry. However, these latter two effects are not completely independent of the bubble phenomena.[a] Consequently, it was difficult to separate out their contribution in these studies.

A number of different types of anodes were examined to study the effects of surface structure on electrochemical impedance. *Cermet inert anodes* freshly fabricated using procedures reported earlier (Strachan et al. 1988) were the focus of the work. These inert anodes were considered representative of the type currently being deployed in larger cells (Strachan et al. 1990) and were compared with the behavior of the other electrodes. *Precorroded cermet inert anodes* that had a rough and highly porous surface layer were tested to determine if a highly porous surface structure influenced the impedance in any way. *Platinum anodes* with four different configurations were tested for comparison with the cermet anodes. Different configurations were employed to address problems associated with changes in cell constant with anode size. Also, comparing effects on horizontal and flat orientations helped determine the source of the anode impedance. *"Platinum brush" anodes* were fabricated and studied to simulate inert anodes with controlled and constant porosity. Similar brush electrodes have been used to determine the effect of surface structure on electrochemical impedance in other systems (de Levie 1964). The relationship between the behavior of planar platinum and

_____

(a) For example, a rough surface will have more hindered bubble flow than a smooth surface. While the roughness itself may contribute to the impedance (perhaps as an area correction), its effect is difficult to distinguish from that of the change in gas flow dynamics that accompanies roughening. This topic is discussed further in Section 4.3.

platinum brush anodes was compared with that between fresh cermet and precorroded cermet anodes to help interpret the role of anode surface structure.

2.0 EXPERIMENTAL PROCEDURE

Experiments were performed using the bench-scale experimental setup shown in Figure 2.1. The electrochemical cell used a three-electrode arrangement including the anode under study as the working electrode, the graphite crucible as the counter electrode, and a reference electrode. The anodes studied included fresh cermet anodes, precorroded cermet anodes, and platinum anodes with various configurations. As shown in Figure 2.2, the configuration for the cermet anodes was a small cylinder with one face exposed to the electrolyte. Four configurations for platinum anodes were evaluated and these are discussed below. A summary of the important characteristics and dimensions of the anodes tested in this study is given in Table 2.1.

The fresh cermet inert anodes were fabricated at PNL (from $NiO/NiFe_2O_4 \cdot$ oxide powder to contain 17% Cu metal by weight) according to procedures discussed in a previous report (Strachan et al. 1988). They were formed into the shape of a small cylinders with a diameter of 1.03 cm. A boron nitride (BN) sheath was used to protect the walls of the anode, allowing only one of its circular faces with an area of 0.84 cm^2 to be exposed to the electrolyte. The face was sanded to a final finish with SiC paper. The connector bar was a Ni rod that had been brazed to the anode during the fabrication procedure as discussed in previous reports (Strachan et al. 1988).

TABLE 2.1. Characteristics of Anodes

Anode	Description of Shape	Area, cm^2
Fresh Cermet	Cylinder with one face exposed.	0.84
Precorroded Cermet	Cylinder with one face exposed.	0.84
Planar Platinum	Rod with one face exposed.	0.077
Platinum Rod	Cylinder with face and sidewalls exposed.	1.00
Platinum Button	"Flat" cylinder with one face exposed.	0.69
Platinum Brush	Bundle of wires with faces exposed.[a]	0.077

(a) This is the macroscopic surface area including the spaces between the wires or the simulated pores. The sum of the areas of the faces of the individual wires, excluding the pores, was 0.062 cm^2.
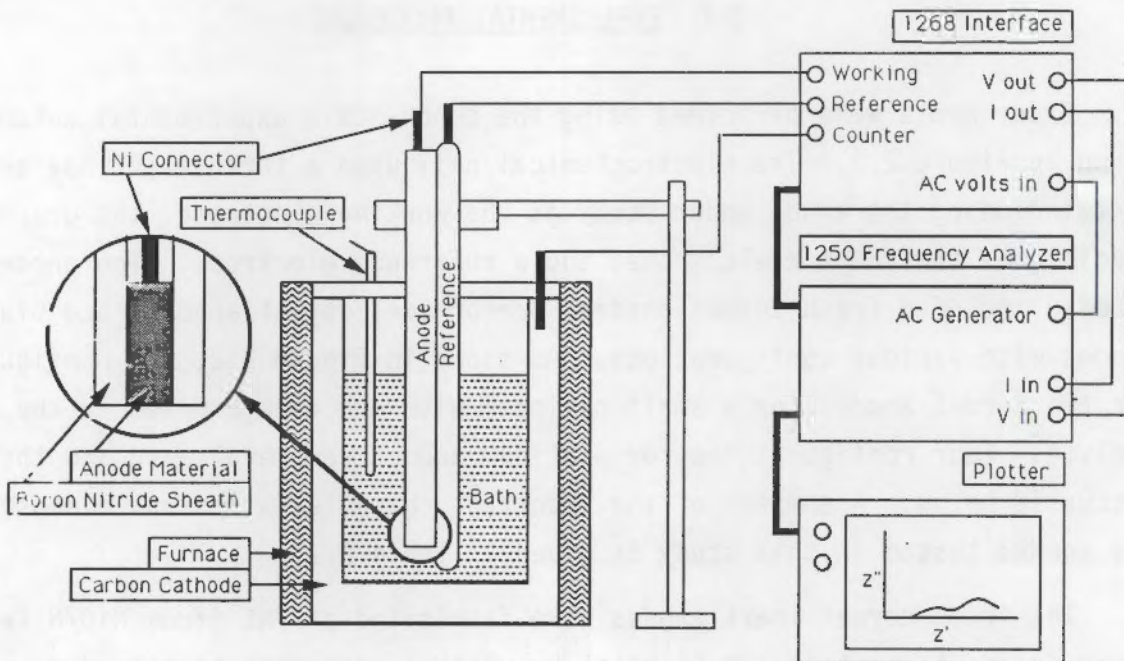
FIGURE 2.1. Apparatus for Electrochemical Impedance Studies.
Exploded view of electrode is shown.
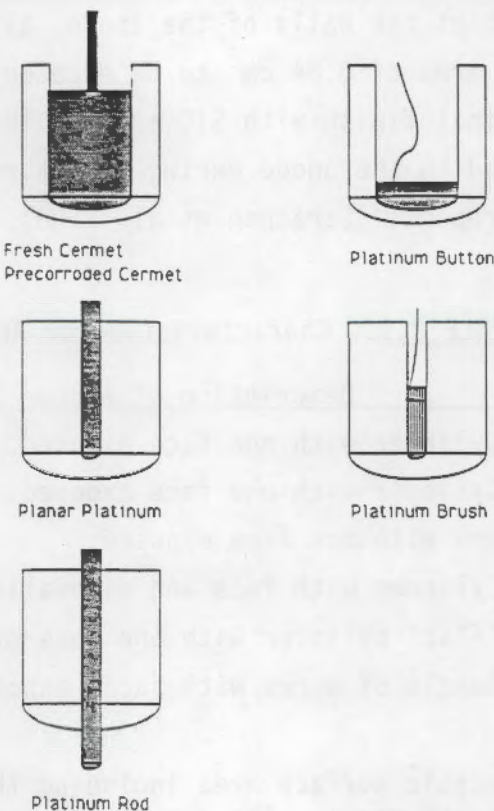
FIGURE 2.2. Various Shapes and Configurations of Anodes Tested

2.2

Precorroded cermet inert anodes were prepared and mounted exactly the same as the fresh cermet anodes but, before testing in this work, were polarized anodically for 1 h at 1 A/cm^2 in a cryolitic bath containing no dissolved alumina. Post-mortem analyses of some of these anodes revealed a >100 μm thick region at the surface that was depleted in copper metal and also very porous.

Platinum anodes with four different configurations were tested. The *planar platinum anode* was prepared from a 0.312-cm-diameter rod obtained from Johnson Matthey, Inc.,[a] and mounted with its terminal face flush with the end of the BN sheath. The *platinum rod anode* was prepared similar to the planar platinum anode and from the same rod stock except that enough circumferential sidewall was left exposed to give a total surface area of 1 cm^2. The *platinum button* anode was prepared from a flat button of platinum with a diameter of 0.94 cm. One side of the button was mounted flush with the BN sheath to give an exposed surface area of 0.69 cm^2. All of the platinum anodes were finished in the same way as the fresh cermet anode, i.e., sanded with 600-grit SiC paper. The *platinum brush* anode was prepared to simulate a surface with a controlled and constant porosity. As shown in Figure 2.3, it consisted of a bundle of 34 wires or bristles each with a diameter of 0.048 cm. The bundle was sheathed in BN, and the exposed surface had the same overall dimensions and appearance as the planar platinum anode except for the open space or *simulated pores* between the platinum wires.

The cathode or counter electrode used in the experiments was a graphite crucible that also served as the cell container. The crucible was large enough to hold about 1 kg of electrolyte. No aluminum metal seed was used in these tests. The reference electrode was the Al/Al$_2$O$_3$ type, fabricated according to a recently published design (Burgman, Leistra, and Sides 1986). The reference electrode was placed at approximately the same position relative to the anode for each test to minimize the effect of differences in cell

---

(a) Johnson Matthey, Inc., Aesar Group, P.O. Box 1087, Seabrook, New Hampshire.

Pt Lead Wire

BN Sheath

Pt Brush
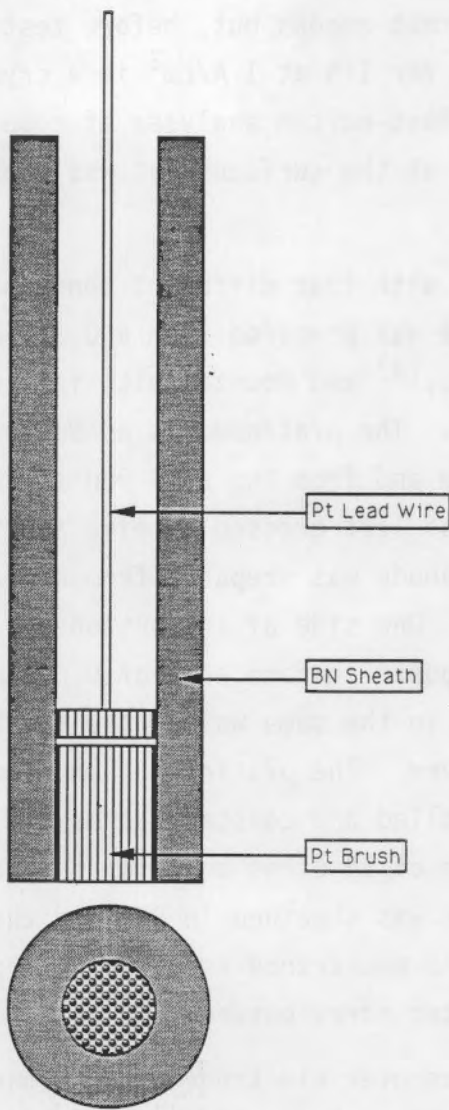
<u>FIGURE 2.3</u>. Schematic of Platinum Brush Anode

geometry on measured anode impedances. The reference electrode was positioned adjacent to the BN sheath and extended about 1/2 in. below the cylindrical face of the anode.

The electrolyte was prepared by mixing appropriate amounts of reagent-grade materials to give a bath ratio equal to 1.15, 5.5% (by weight) CaF_2, 1.0% MgF_2, and 8.0% alumina (saturation). A temperature controller/furnace/thermocouple arrangement was used to melt the raw materials to form a "bath"

and control its temperature at 983 $\pm$2°C. The bath ratio was considered constant and equal to the formulation value (1.15) throughout these short-term tests. The actual variation of bath ratio has been shown to be negligible over the 6-h working life of a laboratory cell (Windisch and Stice 1990b).

Electrochemical impedances were measured at various current densities using a Solartron 1286 Electrochemical Interface and Solartron 1250 Frequency Response Analyzer (FRA).[a] A $\pm$10 mV excitation signal was provided by the FRA and superimposed on the controlling voltage. Three types of electrochemical impedance experiments were performed. In the first type, the frequency of the excitation signal was scanned from 0.1 Hz to 10 kHz using 20 steps per frequency decade. Complex impedance spectra (or plots of the real versus imaginary parts of the complex impedance) were then obtained. These experiments were performed on the fresh cermet inert anodes and on platinum rod anodes. In the second type of experiment, the impedance at 10 kHz was measured for all of the anodes in Table 2.1 as a function of current density (and applied anode potential). The anode potential was set, then the current density and impedance were measured after about 10 min of equilibration. Data were taken during both a stepwise increase and decrease in potential. In the third type of test, the impedance at 10 kHz was measured as a function of time over a 6-h period after applying a potential which gave a current density of 1 A/cm^2. The current density was kept at this value by carefully adjusting the potential throughout the test.

Data at 10 kHz were collected to determine the behavior of the *electrolyte* (or purely resistive component of) impedance only. As shown in Section 3.2, at 10 kHz the contribution of capacitive effects is negligible, particularly at current densities above 0.5 A/cm^2.

(a) Solartron is a tradename of Solartron Instruments, Farmborough, Hampshire, England.

3.0 RESULTS

The impedance data collected in this work included complex impedance spectra, impedance as a function of current density, and impedance as a function of time after applying the controlling voltage.

3.1 COMPLEX IMPEDANCE SPECTRA

The complex impedance spectra[a] for the fresh cermet inert anode at current densities of 0.44 A/cm^2 and 0.80 A/cm^2 are shown in Figures 3.1a and b, respectively. Plots for the platinum rod anode at current densities of 0.53 A/cm^2 and 1.0 A/cm^2 are shown in Figures 3.2a and b, respectively.

The spectra are very similar. Each plot exhibits a loop at low frequencies with a characteristic frequency of about 1 Hz. The diameters of these loops appear to increase with increasing current density, from about 0.07 ohm cm^2 at 0.44 A/cm^2 to 0.10 ohm cm^2 at 0.80 A/cm^2 in the case of the cermet anode, and from approximately 0.10 ohm cm^2 at 0.53 A/cm^2 to 0.15 ohm cm^2 at 1.0 A/cm^2 in the case of the platinum rod anode.

The plots also show some features at higher frequencies (>10 Hz). The high-frequency features were very small and difficult to resolve; however, they are clearer at the lower current density than at the higher current density for both the cermet anode and the platinum rod anode. At the lower current densities they appear to be semicircular. At the higher current densities, the high-frequency features are smaller and obscured (completely, in the case of platinum) by the low-frequency loops.

The high-frequency and low-frequency Z'-intercepts, given by Z'_{hf} and Z'_{lf}, respectively, were estimated by extrapolation from Figures 3.1 and 3.2

(a) Complex impedance spectra are plots of the relationship between the real (Z') and imaginary ($-Z''$) parts of the complex impedance as a function of the frequency of the excitation signal. These spectra are useful in identifying and characterizing the steps in an electrochemical reaction mechanism. See, for example, Bard and Faulkner (1980).
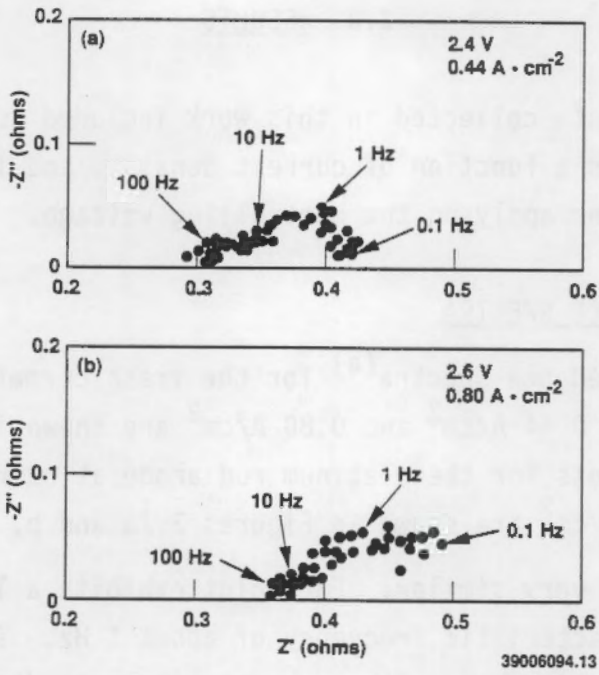
FIGURE 3.1. Electrochemical Impedance Spectra for Fresh Cermet Anode
in Alumina-Saturated Molten Cryolite at 983°C at
(a) 0.44 A/cm² and (b) 0.80 A/cm²
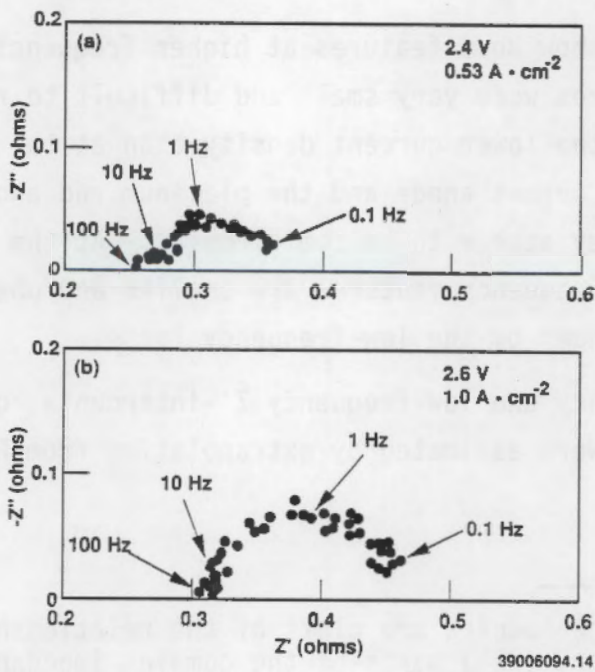
FIGURE 3.2. Electrochemical Impedance Spectra for Platinum Rod Anode
in Alumina-Saturated Molten Cryolite at 983°C at
(a) 0.53 A/cm² and (b) 1.0 A/cm²

and are listed in Table 3.1. As shown in Table 3.1, Z'_{hf} and Z'_{lf} increase with increasing current density for both anodes.

3.2 VARIATION OF IMPEDANCE WITH CURRENT DENSITY

The variation of the real (Z') and imaginary ($-Z''$) parts of the complex electrochemical impedance measured at 10 kHz with respect to current density is shown in Figures 3.3 through 3.8 for the six anodes. Data are given for both forward and reverse sweeps in all cases.

As shown in the figures, Z' is the predominant component of the complex impedance at 10 kHz and the only significant component at current densities near 0.5 A/cm^2 and above. Since 10 kHz is a "reasonably high" frequency according to the complex impedance spectra in Figures 3.1 and 3.2, Z' at 10 kHz can be equated to Z'_{hf} defined in Section 3.1. Near 0.5 A/cm^2 and above, the impedance is largely resistive. At lower current densities, particularly in the case of the platinum anodes, significant contribution from the imaginary or capacitive component, $-Z''$, occurs even at 10 kHz. This may indicate the presence of some stray reactions, possibly the oxidation of carbon particles from the graphite crucible that occur significantly only at low overpotentials.

The variation of Z' with current density followed the same pattern for all of the anodes tested. Under conditions where $-Z''$ is negligible, Z' increased with increasing current density. This trend has been observed in previous studies at PNL (Strachan et al. 1988).

TABLE 3.1. Estimated Z' Intercepts

Anode	Current Density, A/cm^2	Z'_{hf}, ohm cm^2	Z'_{lf}, ohm cm^2
Fresh Cermet	0.44	0.30	0.42
	0.80	0.36	0.50
Platinum Rod	0.53	0.25	0.37
	1.0	0.31	0.46

3.3
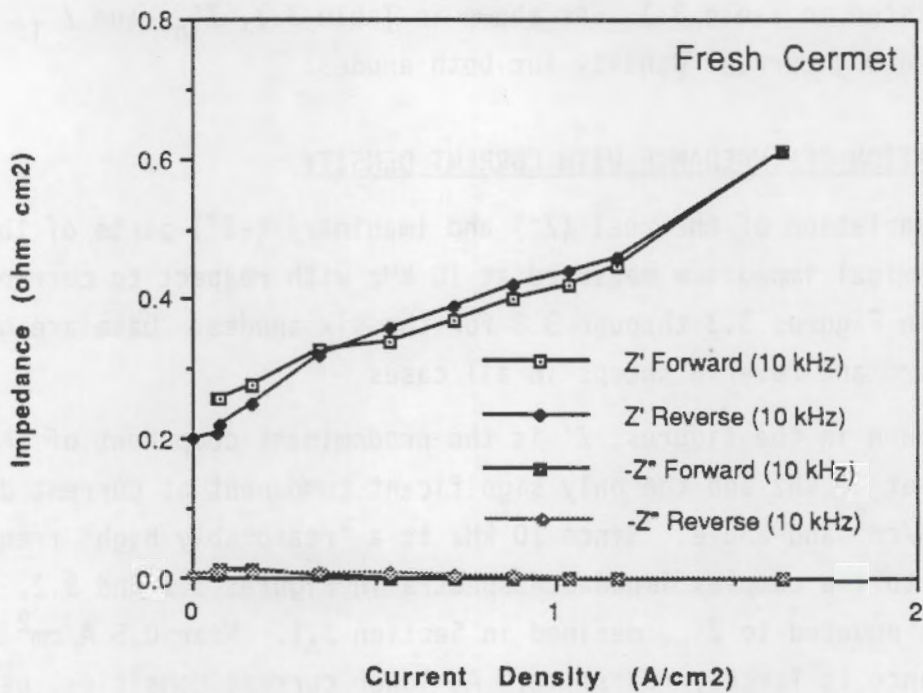
FIGURE 3.3. Impedance as a Function of Current Density
for Fresh Cermet Anode
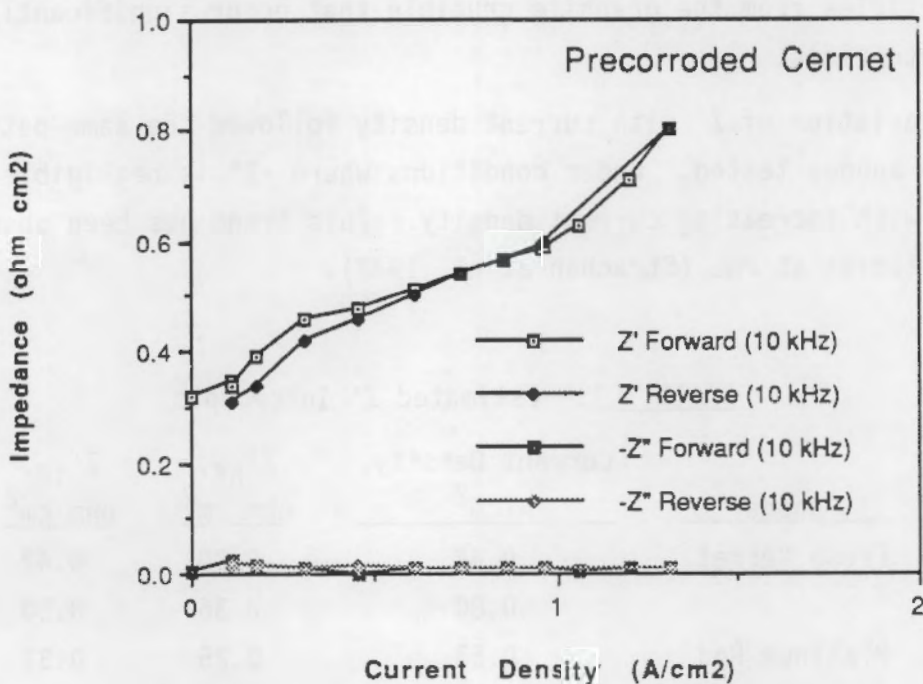
FIGURE 3.4. Impedance as a Function of Current Density
for Precorroded Cermet Anode

3.4
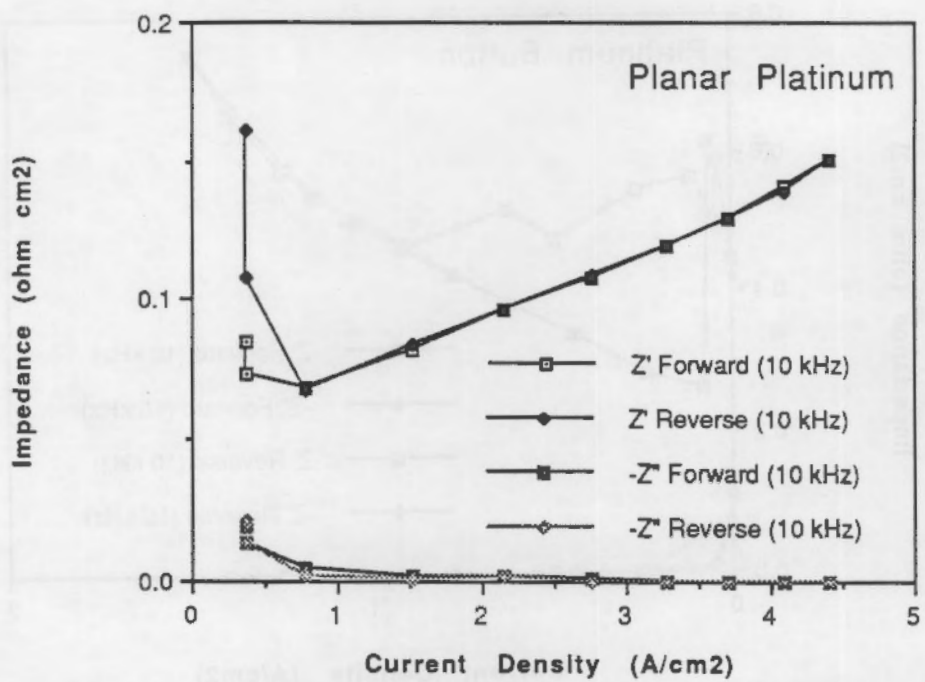
FIGURE 3.5. Impedance as a Function of Current Density for Planar Platinum Anode
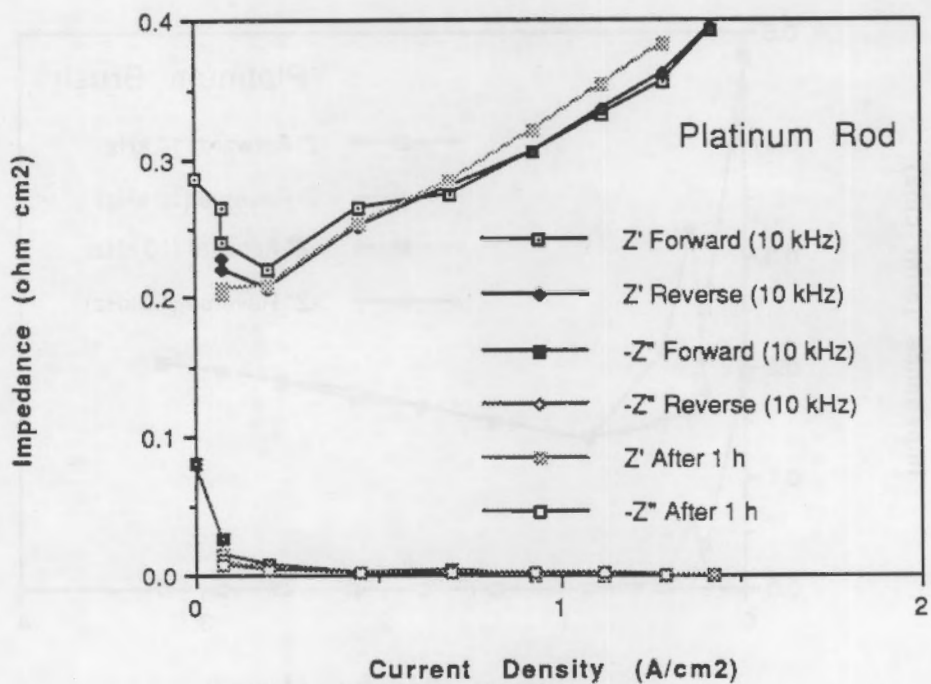
FIGURE 3.6. Impedance as a Function of Current Density for Platinum Rod Anode

3.5
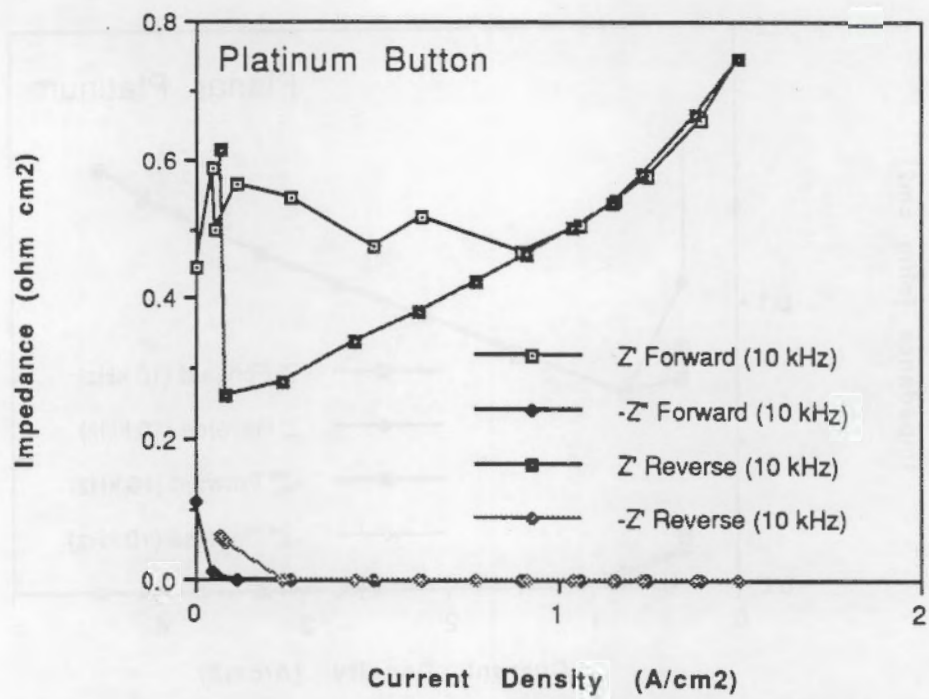
FIGURE 3.7. Impedance as a Function of Current Density for Platinum Button Anode
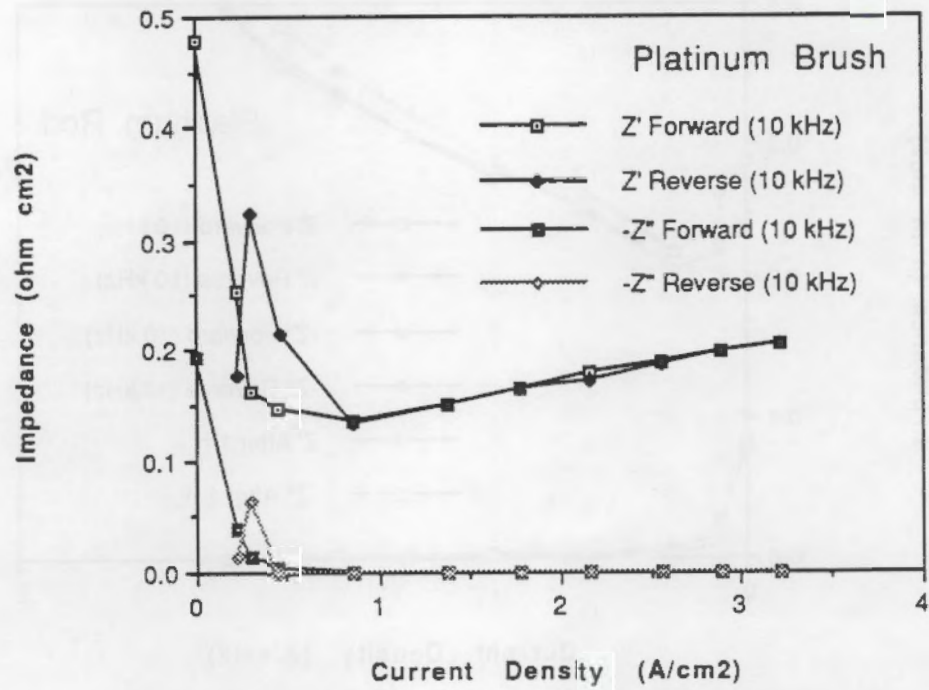
FIGURE 3.8. Impedance as a Function of Current Density for Platinum Brush Anode

The planar platinum and platinum brush anodes showed inordinately low impedances as reflected in the different scales for Figures 3.5 and 3.8. The reason is not certain, but it is not due to materials properties alone since the platinum rod and the platinum button gave impedances more in line with the cermet anodes. More likely, the much smaller surface areas for the planar platinum and platinum brush anodes (about an order of magnitude smaller than the other electrodes, as indicated in Table 2.1) and their placement at slightly different positions with respect to the reference electrode (as a consequence of their different size) contributed to the observed differences in measured impedances. Leakage of small amounts of electrolyte into the crevices between the anode and the BN sheath, while not causing a noticeable perturbation in the case of the large anodes, might have contributed significantly for the small-area anodes.

Thermal expansion of the anodes might have also caused a proportionately greater increase in exposed surface area for the smaller anodes. For example, in the case of the planar platinum electrode, assuming a heat zone of 4 in. at 1000°C, thermal expansion would cause approximately a doubling in exposed surface area. These considerations suggest that the impedances and current densities for the small anodes may be in error because of an error in measuring the exposed surface area. The surprisingly large current densities in Figures 3.5 and 3.8 could also be explained by an error in the surface area measurements. Because of these differences, only electrodes with reasonably similar geometries could be compared reliably. The data for the fresh cermet anode were compared with that for the precorroded cermet anode. The data for the planar platinum anode were compared with that for the platinum brush anode. The platinum rod and platinum button anodes were compared specifically to determine the effects of anode shape on the electrochemical impedance.

Some hysteresis was also observed between the forward and reverse traces in all cases. The hysteresis was more significant for the cermet anodes, the platinum rod, and, particularly, the platinum button than for the planar platinum and platinum brush electrodes. To determine under what conditions hysteresis effects were minimal, impedance data were collected on the platinum rod after polarizing it anodically at 1 A/cm^2 for 1 h. As shown in

Figure 3.6, these data were also slightly different from most of the data collected during the initial forward and reverse traces. However, at current densities around 0.5 A/cm^2, the data after 1 h were very close to data collected during the initial *reverse* trace. Data for Z' near 0.5 A/cm^2 and above taken from the reverse traces for the platinum rod and platinum button anodes are plotted in Figure 3.9. Similar data for the fresh and precorroded cermet anodes are plotted in Figure 3.10. Figure 3.11 shows a similar plot for the planar platinum and platinum brush anodes but over a much wider current density range. In all cases, the plots are very linear. Linear regression analyses were performed, and the results are given in the same figures. The correlation coefficients, R, were very close to 1.000.

As shown in Figure 3.9, the platinum button anode has a much higher impedance than the platinum rod anode at 10 kHz over the current density range plotted. Figure 3.10 shows that the precorroded cermet anode exhibited higher values for Z' than the fresh cermet anode over the current density range plotted, while Figure 3.11 indicates the platinum brush anode gave higher values for Z' than the planar platinum anode.

3.3 VARIATION OF IMPEDANCE WITH TIME

Figure 3.12 illustrates the variation of Z' (measured at 10 kHz) with time over the course of 6 h after a potential step to give a current density of 1 A/cm^2. The current density was maintained at this value by adjusting the polarization voltage. Data are shown for the fresh cermet anode, the precorroded cermet anode, and the platinum rod anode.

As shown in Figure 3.12, after an initial rise in impedance during the first few minutes, the impedance of the fresh cermet anode was fairly constant over the 6-h period. A slight decrease may have begun after 5 h, but it is not certain whether this trend is significant and persistent. In contrast, the precorroded cermet anode showed a steadily increasing impedance over the course of the 6 h, almost doubling in value at the end of the test. The platinum rod anode showed very little variation with time similar to the fresh
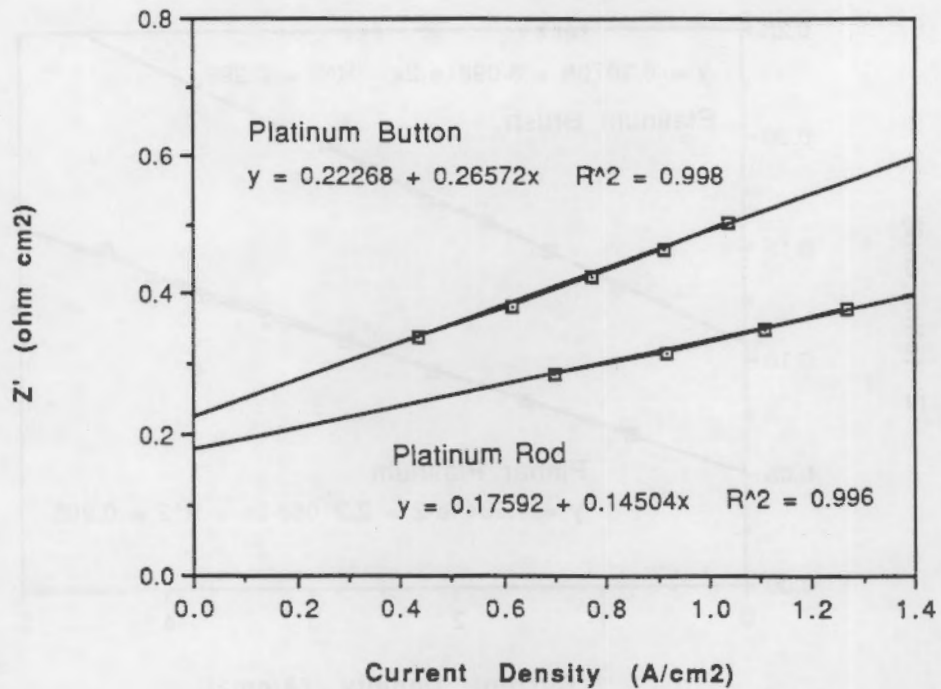
FIGURE 3.9. Linear Regions of Z' Versus Current Density Curves for Platinum Button and Platinum Rod Anodes
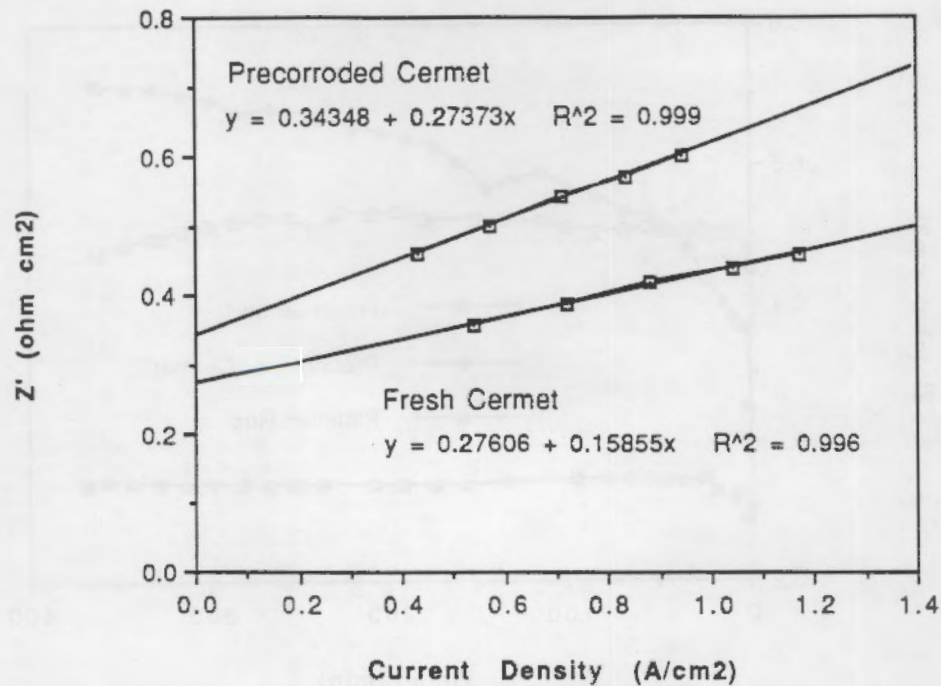
FIGURE 3.10. Linear Regions of Z' Versus Current Density Curves for Fresh Cermet and Precorroded Cermet Anodes

3.9
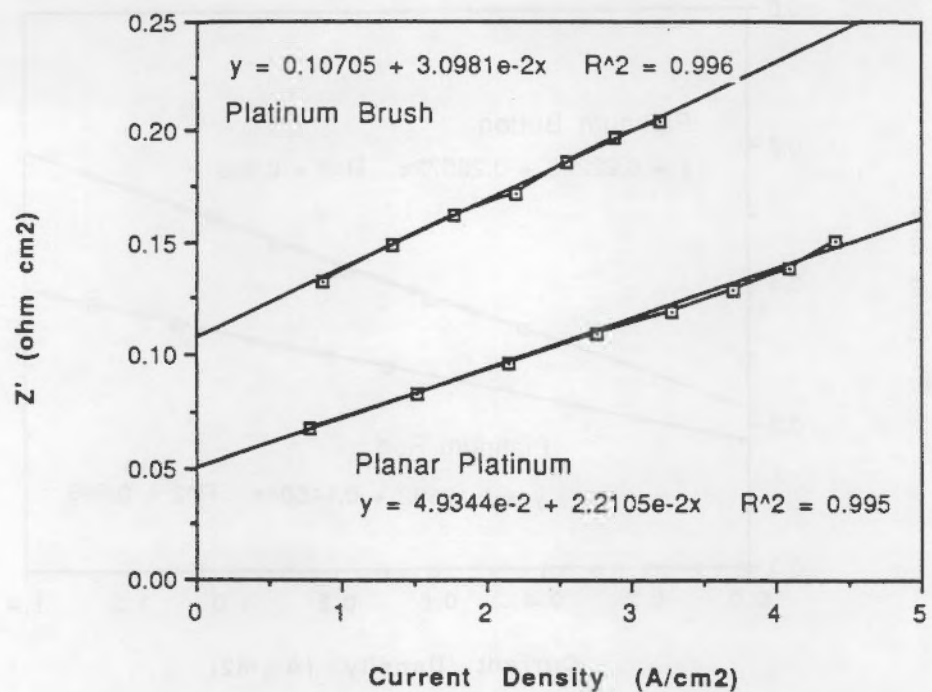
FIGURE 3.11. Linear Regions of Z' Versus Current Density Curves for Planar Platinum and Platinum Brush Anodes
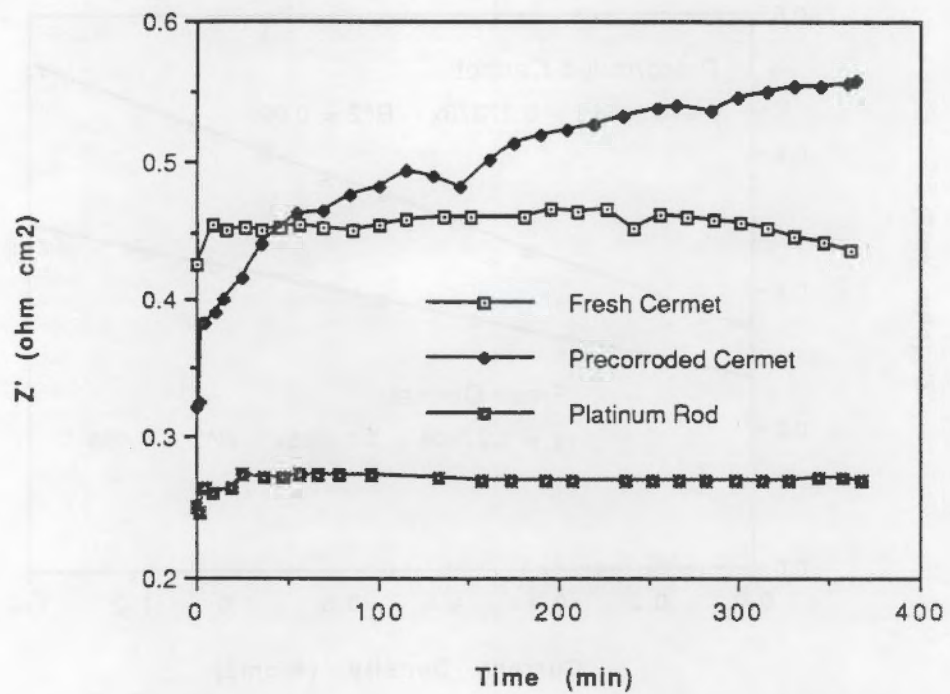
FIGURE 3.12. Variation of Z' with Time for Fresh Cermet, Precorroded Cermet and Platinum Rod Anodes

3.10

cermet; although the absolute magnitude of the impedance was different, probably due to the different shapes of the anodes as discussed in Section 3.2.

correct, although the absolute magnitude of the impedance was different, probably due to the different amount of the anodes as discussed in Section 3.2.

4.0 DISCUSSION

The source of the impedance on the cermet inert anodes was the principal issue under study. Using electrodes of different compositions and configurations, it was possible to determine the factors that contributed to the anode impedance. Unfortunately, the relative importance of each of these factors could not be distinguished since most of them are interrelated. The following approaches for analyzing the data were used: 1) comparing the impedances on the platinum rod and platinum button anodes; 2) characterizing the loops in the electrochemical impedance spectra; 3) comparing the differences in the impedance on fresh cermet anodes and precorroded cermet anodes with differences in impedance on the planar platinum anodes and platinum brush anodes, and observing how the impedance on the various anodes varied with time.

4.1 EFFECT OF ANODE CONFIGURATION

As shown in Figure 3.9, the impedance of the platinum anodes was strongly influenced by the anode configuration. The platinum button anode showed a higher impedance and a higher rate-of-change of impedance with current density (slope) than the platinum rod anode. Since these anodes were identical in composition (both platinum) and had the same surface finish, the differences in impedance behavior may be attributed to the differences in the configuration of the anodes. The two anodes were both cylindrical but had different amounts of horizontally oriented cross-sectional surface and different amounts of vertically oriented cylindrical sidewall exposed to the electrolyte. The platinum rod anode had predominantly sidewall or vertical area, while the platinum button anode had only cross-sectional or horizontal area.

Since the orientation of the surfaces has a strong influence on gas flow, it seems likely that the observed differences in the impedances for the platinum rod and the platinum button anodes arose from the differences in gas flow. A horizontal anode could trap more gas below it than a vertical anode where the gas flow would be relatively unimpeded. The trapped gas would be

4.1

expected to increase the impedance of the anode by replacing a volume of electrolyte by an equivalent volume of more poorly conducting gas. As current density is increased, the amount of gas produced is increased and the impedance would also be expected to increase. This is exactly what was observed, as shown in Figure 3.9. The differences in impedance for the platinum anodes with different configurations suggest that gas bubbles are an important factor in determining the electrochemical impedance of inert anodes.

4.2 COMPLEX IMPEDANCE SPECTRA

The electrochemical impedance spectra provide additional evidence that an important component of the electrochemical impedance is from gas bubbles. Z'_{lf}, the low-frequency intercept for these plots, is the sum of at least three components according to Figures 3.1 and 3.2. These components are Z'_{hf}, the "resistance" of the high-frequency process(es) that give(s) rise to the poorly defined high-frequency loop(s), and the "resistance" of the low-frequency process giving rise to the low-frequency loop. The magnitude of the latter resistance is the diameter of the low-frequency loop.

Z'_{hf} can be equated with the electrolyte resistance, R_e. The voltage drop through the electrolyte was computed for each anode as the product of the current density, I, and R_e. As shown in Table 4.1, the voltage drop through the electrolyte increased with current density for both the fresh cermet anode and the platinum rod anode.

TABLE 4.1. Impedances and Overvoltages for Anodes

Anode	Current (I), A/cm^2	Z'_{hf}, $ohm\ cm^2$	Z'_{lf}, $ohm\ cm^2$	IR_e, V	Slope, V	η V
Cermet	0.44	0.30	0.42	0.13	0.42	0.07
	0.80	0.36	0.50	0.29	0.53	0.11
Platinum	0.53	0.25	0.37	0.13	0.35	0.07
	1.0	0.31	0.46	0.31	0.49	0.09

Plots of IR_e versus I for the platinum rod and fresh cermet anodes are shown in Figure 4.1. Additional Z' data collected at 10 kHz and at other current densities (and discussed in Section 3.2) are also included. The curves are non-linear almost certainly because of the increasing gas volume (from bubbles) at higher current densities. The variation of the voltage drop caused by changes in bubble configuration with current density at a given current density is therefore given by the local slope of the IR_e versus I curve. This slope, which is listed in Table 4.1 for the platinum rod and fresh cermet anodes at the various current densities, is simply the additional resistance associated with the change in bubble configuration accompanying a small change in current density. As shown in Table 4.1, the value for the slope is very close to the magnitude of Z'_{1f} for each of the conditions studied. At a sufficiently low excitation frequency (<1 Hz), the spectra "capture" the effect of the bubble configuration on the overall impedance. The spectra-derived impedances also include contributions from the
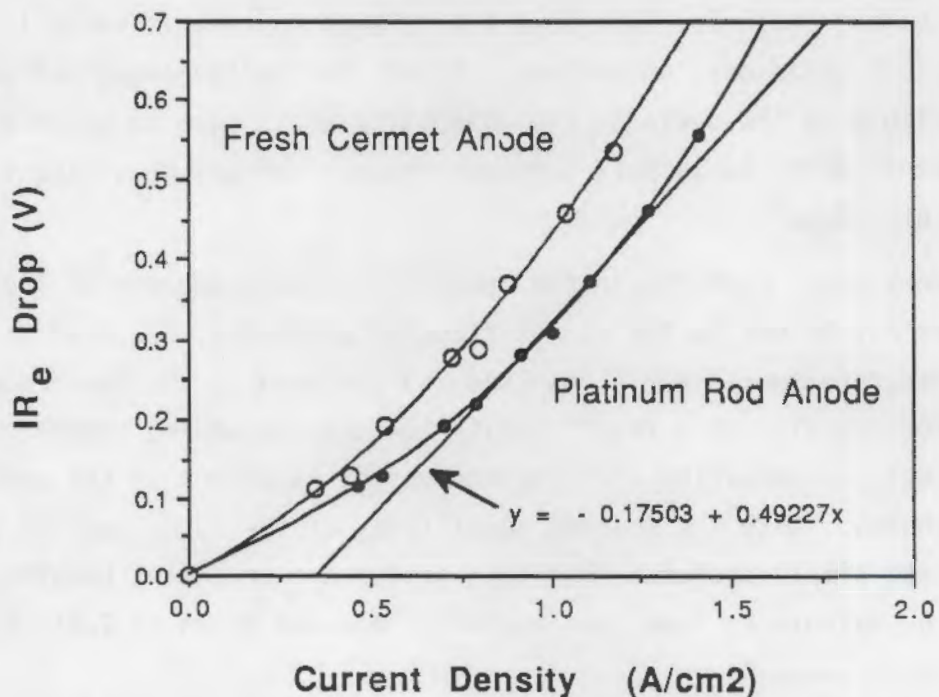
FIGURE 2.3. Variation of the Voltage Drop Through the Electrolyte with Current Density for the Fresh Cermet and Platinum Rod Anodes

electrochemical transformations; but their effects are very small, especially at the higher current densities, as indicated by the size of the high-frequency features in Figures 3.1 and 3.2.

Given the important role the bubble configuration plays in determining the Z_{1f} and, consequently, the dc overpotential, the most likely source of the low-frequency loop is the bubbling process itself. At frequencies significantly above 1 Hz, the bubble configuration is frozen; at frequencies significantly below 1 Hz, the impedance contains an additional "bubble resistance." At intermediate frequencies, the bubble configuration lags behind the current and a loop is obtained.

Other assignments for the low-frequency loop seem implausible. The loop has a "capacitance" on the order of 10^4 $\mu F/cm^2$, which suggests it is not associated with a simple charge-transfer process. The apparent increase in diameter of the low-frequency loop with current density is also inconsistent with a simple Faradaic process, which predicts a resistance inversely proportional to current. The fact that the relaxation time is about 1 s also argues against an adsorption process. Given the limited amount of platinum atoms available on the surface, the adsorption would have to occur at a much faster rate in order to support the experimental current densities that are on the order of 1 A/cm^2.

The very small features in the complex impedance spectra at higher frequencies may be due to the charge-transfer processes, but this is uncertain since the features were poorly resolved and obscured by the low-frequency loop. Unfortunately, this result limits the utility of the electrochemical impedance data in comparing the electrochemical reactions at the cermet and platinum anodes. With the present sensitivity of the technique, it appears that the data simply indicate that both anodes are producing bubbles. Overvoltages, η, calculated from the impedance data and given in Table 4.1,[a] are

_____

(a) The overvoltages were calculated by subtracting the voltage drop through the electrolyte, IR_e, and the decomposition potential for alumina, 2.20 V versus Al/Al_2O_3 (Grjotheim et al. 1982), from the observed anode potential relative to Al/Al_2O_3.

also inconclusive. The values for the overvoltages on platinum differ
significantly from those reported by Thonstad (1968) and, taken together with
the observed differences in the IR_e versus I curves for the platinum and
cermet anodes (Figure 4.1), seem to indicate a dependence on cell geometry,
anode shape and, possibly, anode surface structure (e.g., roughness). This
would not be surprising since the magnitude of the "bubble effect" would also
be expected to vary with these parameters. Studies on carbon anodes have
shown similar effects (Dewing and van der Kouwe 1975). Given the need to keep
power losses as low as possible in large-scale aluminum reduction cells,
particularly in the case of inert anodes where the thermodynamic decomposition
potential is high (relative to carbon anodes), further work would seem
warranted to sort out the roles of these important variables on overvoltage.

4.3. EFFECT OF ANODE SURFACE STRUCTURE

The effects of surface structure are demonstrated in Figure 3.10 and
3.11. As shown in Figure 3.10, the impedances measured at current densities
within the "linear region" are significantly higher for the precorroded cermet
anode than for the fresh cermet anode. For example, at 1.0 A/cm^2 the
impedance is about 50% larger for the precorroded cermet anode than for the
fresh cermet anode. The slope of the curve also appears larger for the pre-
corroded anode but whether this difference is significant or not is unclear
from these data. Comparing the data for the fresh cermet anode in Figure 3.10
with the platinum button anode in Figure 3.9 shows good correlation of the
magnitudes of the impedance measurements within this current density range but
a slight difference in slope.

The larger impedances for the precorroded anode are consistent with
results from other work at PNL (Windisch and Stice 1990b). From these earlier
data it was concluded that the rougher, more porous surface structure of
corroded anodes helped raise the impedance by somehow reducing the amount of
active surface area. In light of the bubble effect proposed in Sections 4.1
and 4.2, the role of roughness is better explained. A rougher surface area
would retard the bubble flow and retain a higher volume of gas at the

4.5

electrode surface. (The effect would be expected to be worse in the case of a horizontal electrode.) The larger gas volume would impart a higher solution resistance and, consequently, a larger Z' at high frequencies.

Despite these arguments, there is a possibility that the higher impedance for the precorroded anode was due to differences in the chemical composition of the surface region. The precorroded anode has a surface region depleted in copper metal and is possibly more resistive. As a way to address the possibility that a resistive reaction layer may have contributed to the impedance, platinum anodes with different configurations were tested. Figure 3.11 shows how the planar platinum anode compared with the platinum brush anode. As shown in Figure 3.11, the impedances were higher for the platinum brush anode than for the planar platinum anode. Since the platinum brush anode differed from the planar platinum anode because it had spaces (between bristles) that were intended to simulate pores, it is reasonable that these simulated pores contributed to the higher impedance.

Exactly how the pores gave rise to a higher impedance is uncertain, but gas bubbles may have been trapped in the spaces and this somehow retarded the flow of the gas across the anode surface. A reduction in the surface area alone (i.e. excluding pores) could not completely explain the differences in impedance since they were greater than 100% at some current densities. In comparison, the "nonpore" surface area for the brush electrode was only 20% less than that of the planar electrode as indicated in the Table 2.1 footnote. It is also significant that the impedances were *greater* for the brush anode than for the planar anode, which indicates that the pores themselves did not contribute additional surface area for electrolysis. Consequently, *significant amounts of oxygen gas appear not to be generated in pores*. Rather, the pores may act as traps for bubbles. The results suggest that the trapped gas not only removes active surface area from the process but impedes the reactions directly, perhaps by changing the dynamics of bubble flow at the electrode surface. Further work is clearly required to sort out the effects of a rough or porous surface on bubble dynamics.

The variation of the impedances with time shown in Figure 3.12 for the fresh and precorroded cermet anodes and for the platinum rod anode also suggests that the factors contributing to the impedance are mostly unchanging for the fresh cermet anode and quite dynamic in the case of the precorroded anode. The behavior of the fresh cermet anode is like platinum, relatively stable with time, suggesting the surface structure of the anode does not significantly change during polarization over the course of 6 h. The increasing impedance of the precorroded anode, however, indicates that a cermet anode, once corroded, may worsen in performance. The effect may be due to an accelerated change in surface structure for the precorroded anode or to a very gradual saturation of the highly porous electrode surface by gas bubbles or electrolyte.

In summary, the impedance data suggest that the surface structure of the anode, i.e., roughness and/or surface porosity, plays an important role in determining the impedance during gas generation. The gas bubbles produced during electrolysis cause an increase in impedance as a function of current density, while the surface structure of the anode appears to influence the magnitude of this effect.

5.0 CONCLUSIONS

The electrochemical impedances of cermet inert anodes in alumina-saturated molten cryolite as a function of frequency, current density, and time indicated that a significant component of the impedance is due to the gas bubbles produced at the anode during electrolysis. Electrochemical impedance spectra exhibited a loop with a characteristic frequency of 1 Hz that was assigned to bubble relaxation. This assignment taken together with the variation of the electrolyte impedance with current density was very strong evidence that bubbles, and not a resistive film, were a primary source of the impedance under dc polarization conditions. Properties previous assigned to such a film are more likely due to the bubbles and those factors that affect the properties and dynamics of the bubbles at the anode surface. Varying the anode surface structure, i.e. porosity and orientation, was observed to influence the impedance and this was related to the effects of changing surface structure on bubble flow.

6.0 REFERENCES

Bard, A. J., and L. R. Faulkner. 1980. _Electrochemical Methods: Fundamentals and Applications_. John Wiley and Sons, Inc., New York.

Burgman, J. W., J. A. Leistra, and P. J. Sides. 1986. "Aluminum/Cryolite Reference Electrodes for Use in Cryolite-Based Melts." _J. Electrochem. Soc_. 133(3):496-500.

de Levie, R. 1964. "On Porous Electrodes in Electrolyte Solutions - IV." _Electrochim. Acta_. 9:1231-1245.

Dewing, E. W., and E. Th. van der Kouwe. 1975. "Anodic Phenomena in Cryolite-Alumina Melts: I. Overpotentials at Graphite and Baked Carbon Electrodes." _J. Electrochem. Soc_. 122(3):358-363.

Grjotheim, K., C. Krohn, M. Malinovsky, K. Matiasovsky, and J. Thonstad. 1982. _Aluminum Electrolysis: Fundamentals of the Hall-Heroult Process_. Aluminum-Verlag, Dusseldorf, Germany.

Strachan, D. M., O. H. Koski, S. C. Marschman, C. H. Schilling, and C. F. Windisch Jr. 1988. _Fiscal Year 1987 Annual Report for the Inert Electrodes Program_. PNL-6746, Pacific Northwest Laboratory, Richland, Washington.

Strachan, D. M., C. F. Windisch, Jr., O. H. Koski, L. G. Morgan, R. D. Peterson, N. E.Richards, and A. T. Tabereaus. 1990. _Results from Electrolysis Test of a Prototype Inert Anode_. PNL-7345, Pacific Northwest Laboratory, Richland, Washington.

Thonstad, J. 1968. "Anodic Overvoltage on Platinum in Cryolite-Alumina Melts." _Electrochim. Acta_. 13:449-456.

Tobias, C. W. 1959. "Effect of Gas Evolution on Current Distribution and Ohmic Resistance in Electrolyzers." _J. Electrochem. Soc_. 106(9):833-838.

Windisch, C. F., Jr., and N. D. Stice. 1990a. _Characterization of the Reaction Layer or Film on PNL Inert Anodes: Progress Report for April-December 1989_. PNL-7326, Pacific Northwest Laboratory, Richland, Washington.

Windisch, C. F., Jr., and N. D. Stice. 1990b. _Final Report on the Characterization of the Film on Inert Anodes_. PNL-7589, Pacific Northwest Laboratory, Richland, Washington.

Zuka, S., C. Herdlicka, and M. Terzi. 1980. "On Porosity-Overvoltage Correlation for Carbon Anodes in Cryolite-Alumina Melts." _Electrochim. Acta_. 25:211-216.

DISTRIBUTION

No. of
Copies

No. of
Copies

OFFSITE

M. J. McMonigle
U.S. Department of Energy
Office of Industrial Programs
Forrestal Building
Washington, DC 20585

P. H. Salmon-Cox
U.S. Department of Energy
Office of Industrial Programs
Forrestal Building
Washington, DC 20585

12 DOE Office of Scientific and
Technical Information

C. Anderson
Columbia Aluminum Co.
85 John Day Dam Road
Goldendale, WA 98620

J. V. Anderson
WCVE3
EG&G Idaho, Inc.
Idaho Falls, ID 83415

D. Auburg
Bonneville Power
   Administration
P.O. Box 3621, PDX 97208
Portland, OR 97208

F. W. Baker
Ceramics Division
Alcoa Laboratories
Alcoa Center, PA 15069

M. Baltzell
Eastalco Aluminum Company
Alumax, Inc.
5601 Manor Woods
Frederick, MD 21701

J. A. Barclay
U.S. Bureau of Mines
2401 "E" Street N.W.
Washington, DC 20241

H. Robert Baumgartner
Ceramics Division
Alcoa Laboratories
Alcoa Center, PA 15069

T. R. Beck
Electrochemical Technology
   Corp.
1601 Dexter Avenue
Seattle, WA 98109

S. Berwagan
Bonneville Power
   Administration
P.O. Box 3621 K
Portland, OR 97208

T. M. Besmann
Metals and Ceramics Division
Oak Ridge National Laboratory
P.O. Box X, Bldg. 4515
Oak Ridge, TN 37831-6063

K. A. Blakely
President
Advanced Refractory
   Technologies, Inc.
699 Hertel Ave.
Buffalo, NY 14207

M. H. Blenk
Du Pont
P.O. Box 787
Niagara Falls, NY 14302

L. G. Boxall
Martin Marietta Laboratories
1450 South Rolling
Baltimore, MD 21227

J. Bracher
Kaiser Aluminum and Chemical
  Corp.
825 N.E. Multnomah St.,
  Suite 960
Portland, OR 97232-2150

R. Brandt
Department of Materials
  Science and Engineering
University of Washington FB-10
Seattle, WA 98195

J. J. Brown, Jr.
Materials Engineering
Virginia Polytechnic Institute
Blacksburg, VA 24061

A. Budner
Bonneville Power
  Administration
P.O. Box 3621--EPA
Portland, OR 97208

A. J. Caputo
Development Division
Oak Ridge Y-12 Plant
Building 9202 MS-8095
Oak Ridge, TN 37831-8095

N. Clark
Bonneville Power
  Administration
Industrial Conservation
P.O. Box 3621
Portland, OR 97208

A. Cooke
Martin Marietta Laboratories
1450 South Rolling
Baltimore, MD 21227

J. A. Coppola
Standard Oil Engineered
  Materials Company
P.O. Box 156
Niagara Falls, NY 14302

Business Expansion
  Division Library
Washington State Dept of Trade
  Business Expansion Library
2001 6th Avenue # 2700
Seattle, WA 98121-2522

R. Curtis
Materials Development
  Corporation
81 Hicks Avenue
Medford, MA 02155

J. V. Day
Kaiser Aluminum and Chemical
  Corp
E2111 Hawthorne Road
Mead, WA 99021

D. H. DeYoung
Alcoa Technical Center
Alcoa Center, PA 15069

S. Diamond
Battelle Columbus Laboratories
505 King Avenue
Columbus, DH 43201-2693

C. W. Doerr
The Stackpole Corporation
Cermag Division
201 Stackpole Street
St. Marys, PA 15847

T. Dwonch
Snake River District
BPA
101 W. Poplar
Walla Walla, WA 99362

G. L. Eitel
Stone & Webster Engineering
  Corp.
Greenwood Plaza Box 5406
Denver, CO 80217

R. Engdahl
Deposits and Composites, Inc.
318 Victory Drive
Herndon, VA 22070

J. F. Elliott
MIT
Room 4-138
77 Massachusetts Avenue
Cambridge, MA 02139

B. G. Epstein
A. D. Little, Inc.
955 Lenfant Plaza SW 4200
Washington, DC 20024-2119

J. W. Evans
University of California
Dept of Matl. Sci. and Mineral
  Eng.
Berkeley, CA 94720

R. A. Fenimore
ICI Advanced Materials
Rollins Building, Eighth Floor
Wilmington, DE 19897

D. A. Figgins
ARCO Petroleum Products Co.
P.O. Box 61004
Anaheim, CA 92803-6104

P. Foster
Alcoa Laboratories
P.O. Box 772
New Kensington, PA 15068

J. Gee
Great Lakes Research Corp
P.O. Box 1031
Elizabethton, TN 37643

T. Gilligan
Eltech Systems Corp.
625 East Street
Fairport Harbor, OH 44077

W. M. Goldberger
Superior Graphite Co.
120 S. Riverside Plaza
Chicago, IL 60606

J. Goodwell
Center for Metals Production
Mellon Institute
4400 Fifth Avenue
Pittsburgh, PA 15213

J.A.S. Green
Martin Marietta Laboratories
1450 South Rolling
Baltimore, MD 21227

C. Griffin
Ceramatec Inc.
2425 S. 900 West
Salt Lake City, UT 84119

L. I. Grindstaff
Great Lakes Research Corp.
P.O. Box 1031
Elizabethon, TN 37643

J. Haggerty
MIT
Building 12, Room 009
77 Massachusetts Avenue
Cambridge, MA 02139

I. L. Harry
Electric Power Research
  Institute
P.O. Box 10412
Palo Alto, CA 94303

W. E. Haupin
2820 7th Street Road
Lower Burrell, PA 15068

R. Hill
Union Carbide Corp.
P.O. Box 94637
Cleveland, OH 44101

H. F. Hillegass
Alcoa Wenatchee Works
P.O. Box 221
Wenatchee, WA 98807

D. G. Howitt
College of Engineering
University of California,
  Davis
Davis, CA 95616

F. R. Huettig
Advanced Magnetics, Inc.
45 Corey Lane
Mendham, NJ 07945

G. R. Hyde
U.S. Bureau of Mines
2401 "E" Street N.W.
Washington, DC 20241

S. C. Jacobs
Primary Processing
Aluminum Company of America
Alcoa Technical Center
Alcoa Center, PA 15069

S. H. Jan
Tennessee Valley Authority
R&D Division - MR 3A
Chattanooga, TN 37401

N. Jarrett
149 Jefferson Avenue
New Kinsington, PA 15068

J. Johnson
Intalco Aluminum Company
P.O. Box 937
Ferndale, WA 98248

M. H. Johnson
Alcoa Wenatchee Works
P.O. Box 1031
Elizabethon, TN 37643

L. Joo
Great Lakes Research Corp
P.O. Box 1031
Elizabethon, TN 37643

M. Karmous
Oregon State Department of
  Energy
625 Marion Street, N.E.
Salem, OR 97310

R. Keller
RD 3 Roundtop Road
Export, PA 15632

K. Krupinski
Mail Stop 57
U.S. Steel Technical Center
1 Technical Center Drive
Monroeville, PA 15146

G. Y. Lai
Cabot Corporation
P.O. Box 9013
Kokomo, IN 46902-9013

R. A. Landy
Director of Research
North American Refractories
  Co.
3127 Research Dr.
State College, PA 16801

J. E. Lane
Ceramic Research and
  Development Center
Westinghouse Electric
  Corporation
1310 Beulah Road
Pittsburgh, PA 15235

Sai-Kwing Lau
Standard Oil Engineered
  Materials Company
Niagara Falls R&D Center
P.O. Box 832
Niagara Falls, NY 14302

J. J. Leddy
Dow Chemical U.S.A.
1776 Building
Midland, MI 48640

W. W. Liang
Gas Research Institute
8600 West Bryne Mawr Avenue
Chicago, IL 60631

W. H. Link
Columbia Aluminum Corp.
85 John Day Dam Road
Goldendale, WA 98620

Steve Loftness
Washington State Energy Office
400 E. Union
Olympia, WA 98504

W. Long
Building B815
Dow Chemical
Freeport, Texas 77541

A. G. Longmuir
Kaiser Aluminum and Chemical
  Corp.
P.O. Box 877
Pleasonton, CA 94566

R. A. Lowden
Metals and Ceramics Division
Oak Ridge National Laboratory
P.O. Box X, Bldg, 4515
Oak Ridge, TN 37831-6063

W. N. Maclay
Koppers Company, Inc.
1005 William Pitt Way
Pittsburgh, PA 15238-1336

J. C. McCloskey
Ten Mile River Associates
296 Mt. Hope Street
North Attleboro, MA 02760

S. C. Manaktala
Manager of Technology
Reduction Division
Kaiser Aluminum and Chemical
  Corp
300 Lakeside Drive
Oakland, CA 94643

V. H. Markant
Du Pont
P.O. Box 787
Niagara Falls, NY 14302

C. J. McMinn
Extractive Metallurgical
  Department
Reynolds Metals Company
P.O. Box 1200
Sheffield, AL 35660

C. H. McMurtry
Standard Oil Engineered
  Materials Company
Niagara Falls R&D Center
P.O. Box 832
Niagara Falls, NY 14302

M. A. Mitnick
Avco Specialty Materials
Subsidiary of Textron Inc.
2 Industrial Avenue
Lowell, MA 01851

H. Mortensen
R. Palika
Cercom, Inc.
P.O. Box 70
Vista, CA 92083

B. C. Mutsuddy
Battelle Columbus Division
505 King Avenue
Columbus, OH 43201-2693

P. Ness
Washington State Dept of Trade
  and Economic Development
2001 6th Avenue #2600
Seattle, WA 98121-2522

A. N. Patel
Battelle Columbus Laboratories
505 King Avenue
Columbus, OH 43201-2693

J. R. Payne
Kaiser Aluminum and Chemical
  Corp.
P.O. Box 877
Pleasanton, CA 94566

T. Payne
Columbia Falls Aluminum Co.
Columbia Falls, MT

W. Pebley
Oregon Freeze Dry Corp.
525 25th Avenue SW
P.O. Box 1048
Albany, OR 97321

K. Peterson
Columbia Aluminum Corp.
85 John Day Dam Road
Goldendale, WA 98620

R. D. Peterson
Reynolds Metals Company
P.O. Box 1200
Sheffield, AL 35660

T. R. Pritchett
Kaiser Aluminum and Chemical
  Corp.
P.O. Box 877
Pleasanton, CA

W. W. Pritsky
Aluminum Association
900 19th St. N.W.
Washington, DC 20006

S. P. Ray
Alcoa Technical Center
Alcoa Center, PA 15069

J. F. Rhodes
Advanced Composite Materials
  Corp.
1525 S. Buncomb Rd.
Greer, SC 29651

N. E. Richards
Reduction Laboratory
Reynolds Aluminum Corporation
P.O. Box 1200
Sheffield, AL 35660

J. J. Ritter
Ceramics Division
National Bureau of Standards
Gaithersburg, MD 20899

R. C. Rohwedder
3028 Ohio Street
Longview, WAD. R. Sadoway
MIT
Room 8-109
77 Massachusetts Avenue
Cambridge, MA 02139

W. Scott
Department of Materials
  Science & Engineering
Wilcox Hall FB-10
University of Washington
Seattle, WA 98195

D. R. Secrist
Great Lakes Research Corp.
P.O. Box 1031
Elizabethon, TN 37643

A. B. Shah
Noranda Aluminum, Inc.
P.O. Box 70
New Madras, MO 63869

No. of
Copies

No. of
Copies

N. Shelton
Intalco
1300 S. W. 5th, Suite 3508
Portland, OR 97201

Brian Spector
Pace Consultants
4848 Loop Central Drive
Houston, TX 77081

F. W. Spillers
Dow Chemical U.S.A.
B-1210 Building
Freeport, TX 77541

Dr. Richard M. Spriggs
Office of the Director
Center for Advanced
  Ceramic Technology
Alfred University
Alfred, NY 14802

D. V. Stewart
Reynolds Metals Co.
P.O. Box 1200
Sheffield, AL 35660

D. Strahan
Reynolds Metals Company
P.O. Box 27003
Richmond, VA 23261

A. T. Tabereaux
Reynolds Metals Company
P.O. Box 1200
Sheffield, AL 35660

G. P. Tarcy
Aluminum Company of America
Alcoa Technical Center
Alcoa Center, PA 15069

P. Thaure
Primary Planning and
  Production Alumax
400 S. El Camino Rd.
San Mateo, CA 94402

W. H. Thielbahr
Conservative Technology
  Division
DOE-Idaho Operations Office
785 DOE Place
Idaho Falls, ID 83402

S. Thomson
General Manager
Klickitat PUD
1313 S. Columbus
Goldendale, WA 98620

R. Unger
Merner Research
P.O. Box 248
Ridgewood, NJ 07451A. Vinnard
Bonneville Power
  Administration (KWI)
P.O. Box 3621
Portland, OR 97208

T. Von Muller-KWI
Bonneville Power
  Administration
P.O. Box 3621
Portland, OR 97208

D. H. Weinblatt
AIMCOR
One Parkway North
Deerfield, IL 60015

J. D. Weyand
EG&G Idaho, Inc.
Idaho Falls, ID 83415

B. Wilcox
Northwest Aluminum Co.
3313 W. Second St.
The Dalles, OR 97058

C. B. Wilson
Dow Chemical U.S. A.
Texas Operations
B-101 Building
Freeport, TX 77541

J. C. Withers
Keramont Research Corporation
4233 S. Fremont Avenue
Tucson, AZ   85714

W. A. Zdaniewski
Engelhard Corporation
Menlo Park, CN 28
Edison, NJ   08818

FOREIGN

D. Brodie
Comalco Ltd.
55 Collins St.
Melbourne, AUSTRALIA

H. Connor
Group Licensing Controller
Johnson Matthey, plc
New Garden House
78 Hatton Garden
London EC1N 8JP   ENGLAND

L. Dion
Alcan International Limited
C.P. 6090
Montreal, Quebec
CANADA, H3C 3H2

T. Kjar
Comalco Ltd.
55 Collins St.
Melbourne, AUSTRALIA

E. W. Dewing
Alcan International
P.O. Box 8400
Kingston, Ontario
CANADA K7L 4Z4

D. N. MacMillan
Alcan International
C.P. 1250
Jonquieve, Quebec
CANADA G7S 4K8

J. H. Reimers
Jan H. Reimers and Associates
   Inc.
221 Lakeshore Road East
Oakville, Ontario
CANADA, L6J 1H7

A. Oye
Institute of Inorganic
   Chemistry
Norwegian Institute of
   Technology
University of Trondheim
N-7034 Trondheim-NTH, NORWAY

J. Thonstad
Laboratories of Industrial
   Electrochemistry
Norwegian Institute of
   Technology
University of Trondheim
N-7034 Trondheim-NTH, NORWAY

K. O. Vee
ASV Ardal Verk
N-5875 Ardalstargen, NORWAY

Dr. Eric Frazer
CSIRO Australia
Division of Mineral Products
339 Williamstown Road
P.O. Box 124
Port Melbourne, Vic 3207

No. of
Copies

ONSITE

    DOE - Richland Operations
    Office

    R. B. Goranson

25 Pacific Northwest Laboratory

    M. Clement
    N. C. Davis

No. of
Copies

    D. K. Hilliard
    G. L. McVay
    N. L. Moore
    L. G. Morgan (10)
    C. H. Schilling
    D. M. Strachan
    R. E. Westerman
    C. F. Windisch
    Publishing Coordination
    Technical Report Files (5)